

Structure and Dynamics of Liquid Water from *ab Initio* Molecular Dynamics—Comparison of BLYP, PBE, and revPBE Density Functionals with and without van der Waals Corrections

I-Chun Lin,^{†,||} Ari P. Seitsonen,^{*,‡} Ivano Tavernelli,[§] and Ursula Rothlisberger[§]

[†]Department of Chemistry, New York University, 100 Washington Square East, New York, New York 10003, United States

[‡]Physikalisch-Chemisches Institut, University of Zurich, Winterthurerstrasse 190, CH-8057 Zurich, Switzerland

[§]Laboratory of Computational Chemistry and Biochemistry, Ecole Polytechnique Fédérale de Lausanne, CH-1015 Lausanne, Switzerland

Supporting Information

ABSTRACT: We investigate the accuracy provided by different treatments of the exchange and correlation effects, in particular the London dispersion forces, on the properties of liquid water using *ab initio* molecular dynamics simulations with density functional theory. The lack of London dispersion forces in generalized gradient approximations (GGAs) is remedied by means of dispersion-corrected atom-centered potentials (DCACPs) or damped atom-pairwise dispersion corrections of the C_6R^{-6} form. We compare results from simulations using GGA density functionals (BLYP, PBE, and revPBE) with data from their van der Waals (vdW) corrected counterparts. As pointed out previously, all vdW-corrected BLYP simulations give rise to highly mobile water whose softened structure is closer to experimental data than the one predicted by the bare BLYP functional. Including vdW interactions in the PBE functional, on the other hand, has little influence on both structural and dynamical properties of water. Augmenting the revPBE functional with either damped atom-pairwise dispersion corrections or DCACP evokes opposite behaviors. The former further softens the already under-structured revPBE water, whereas the latter makes it more glassy. These results demonstrate the delicacy needed in describing weak interactions in molecular liquids.

1. INTRODUCTION

Water is one of the most important chemical substances. The strength and the directional nature of hydrogen bonds (H-bonds) lead to complex cooperative phenomena, as implied by the complicated phase diagram of ice and a long list of anomalies in the properties of liquid water. Despite extensive studies, understanding the microscopic nature of water remains a challenge. Indeed, in spite of the fact that ever more sophisticated experimental and theoretical techniques are applied to study this intriguing medium, the debate is far from being concluded.

Because of its favorable performance-to-cost ratio, the Kohn–Sham formalism of density functional theory (DFT)^{1,2} has emerged as the electronic structure method of choice for many problems in the fields of chemistry, condensed matter physics, and materials science. In spite of the generally good performance, extensive assessments of the parameters used in *ab initio* molecular dynamics (AIMD) simulations of water indicate that the performance of DFT with generalized gradient approximation (GGA) exchange–correlation (XC) functionals on this intriguing system is less than satisfactory. GGA functionals such as BLYP^{3,4} and PBE⁵ predict energetics of water clusters reasonably well. The simulated liquid, however, is overstructured and less dense, and it diffuses too slowly compared with experimental results.^{6–10}

It is essential to realize that interactions in liquid water are not simply H-bonding only but are rather a fine balance between strongly directional H-bonding and nondirectional van der Waals (vdW) interactions, in particular the London

dispersion forces.^{11–13} The deficiency of many approximate exchange–correlation functionals in describing these weak interactions will certainly contribute to the aforementioned discrepancy. In addition, a proper description of vdW interactions is an important prerequisite to gain insight into the influence of hydrophobic effects on the structure and function of specific amino acids, water in zeolites, or fluid flow in carbon nanotubes, to name just a few.

Recently, we have reported how incorporating vdW interactions into DFT–GGA improves the properties of liquid water predicted by AIMD simulations (e.g., a softer structure and an increase in the diffusivity).¹⁴ Later studies from several groups have confirmed this conclusion and shown that the estimated density is also significantly improved.^{15–19} One recent study has also demonstrated that the deficiency of GGA functionals could be reproduced by damping to zero the tail of the Lennard–Jones R^{-6} term in a parametrized force field,¹⁹ substantiating the important role played by vdW interactions in this delicate medium. Furthermore, by dividing the potential of the SPC/E water model into short- and long-range parts, Remsing et al.²⁰ indicate that vdW attractions play the role of a cohesive energy needed to achieve the high density in SPC/E water at low pressure.

Special Issue: Wilfred F. van Gunsteren Festschrift

Received: March 5, 2012

Published: May 29, 2012



In this paper, we go beyond our earlier¹⁴ Car–Parrinello molecular dynamics²¹ studies on liquid water by using not only different treatments of vdW interactions but also several GGA exchange–correlation functionals, i.e., the BLYP, PBE, and revPBE²² functionals. In addition, we have carried out longer simulations for better statistics. We treat the lack of vdW interactions by including either effective dispersion-corrected atom-centered potentials (DCACPs)²³ or damped atom-pairwise dispersion corrections of the C_6R^{-6} form.^{24,25} Developing an efficient way to accurately describe vdW interactions in DFT is still in its infancy, and these two pragmatic schemes offer a good compromise between accuracy and computational cost. Besides structural (radial and angular distribution functions) and dynamical (H-bond statistics, mean squared displacements, self-diffusion coefficients, and orientational autocorrelation functions) properties of liquid water, we also study the properties of small water clusters in order to understand the amount of the contributions from the hydrogen bonding and vdW corrections. The accuracy in the descriptions of both the small water clusters and the liquid form is also relevant when developing force fields that are transferable between both systems.

2. COMPUTATIONAL DETAILS AND METHODS OF ANALYSIS

Simulations are carried out using the CPMD code²⁶ with Goedecker–Teter–Hutter pseudopotentials;²⁷ a plane-wave cutoff of 125 Ry; and the BLYP,^{3,4} PBE,⁵ and revPBE²² functionals. We adopt two sets of empirical vdW corrections (taken from refs 24 and 25, respectively). Oxygen and hydrogen DCACPs for BLYP and PBE are taken from ref 28, and DCACPs for revPBE are calibrated using the same procedure. For ease of comparison, all DCACP parameters used are tabulated in Table 1. The strength σ_1 and the spatial

Table 1. DCACP Parameters for Hydrogen and Oxygen

	BLYP		PBE		revPBE	
	σ_1 [10^{-4} Ha]	σ_2 [Bohr]	σ_1 [10^{-4} Ha]	σ_2 [Bohr]	σ_1 [10^{-4} Ha]	σ_2 [Bohr]
H	−4.06	2.71	0.50	2.47	−20.75	1.70
O	−7.92	2.57	−6.47	1.73	−11.61	2.09

extent σ_2 of DCACPs are similar for all functionals in the case of oxygen. The σ_1 of hydrogen, however, varies widely. For BLYP, it is about half of the value of that for oxygen, and it is almost negligible (but positive) for PBE. But for revPBE, its value is very large, exceeding the value for oxygen by a factor of 2. We note that the same procedure was used for the determination of all the coefficients, and we shall see what the consequence is of the anomalously large coefficient for hydrogen with revPBE.

*-DCACP, *-D_{G2}, and *-D_{WM} denote simulations using functionals augmented with DCACPs, empirical vdW corrections due to Grimme,²⁴ and empirical vdW corrections due to Williams and Malhotra.²⁵ We want to clarify that the results marked as “BLYP-D” in ref 14 have been obtained using the BLYP-D_{WM} scheme.

Simulations of the liquid state are carried out in a cubic 12.42³ Å³ periodic box containing 64 water molecules, corresponding to a density of 1 g/cm³ of light water. To reduce the nuclear quantum effects, the mass of hydrogen is replaced with the one of deuterium. Car–Parrinello molecular

dynamics simulations with a fictitious electron mass of 600 au and a time step of 4 au = 0.097 fs are carried out in the NVE ensemble. The lengths of the trajectories range from 50 to 117 ps. The first 10 ps are treated as the equilibration stage. No thermostat is applied on either the fictitious electronic or the ionic degrees of freedom. Configurations are saved every 10 steps for analysis.

Details about the trajectories are given in the Supporting Information. The small time step and fictitious electron mass have allowed for long and stable simulations without introducing a considerable energy exchange between the ionic and electronic degrees of freedom. No significant drift in the conserved energy is observed (it is less than 0.2 meV ps^{−1}), and the drift in the fictitious electron kinetic energy is no more than 15 meV ps^{−1}. There are, however, small systematic drifts in the ionic temperatures (between 0.1 and 0.6 K ps^{−1}) in the revPBE-D_{G2} run and all BLYP- and PBE-based simulations.

Since the simulations are carried out in the NVE ensemble, the average temperature of each simulation is slightly different. For a fair comparison, we scale the maximum (g_{OO}^{\max}) and minimum (g_{OO}^{\min}) of the oxygen–oxygen radial distribution function (g_{OO}) using the relation proposed in ref 29, $-dg_{OO}/dT = \text{constant}$. The corresponding constants (9.0×10^{-3} and -2.7×10^{-3} K^{−1} for g_{OO}^{\max} and g_{OO}^{\min} , respectively) are obtained by fitting to TIP4P-pol2 results.³⁰ We calculate the coordination number of water molecules, n , by integrating g_{OO} up to the first minimum. Furthermore, we use the definition of ref 31 for H-bond analysis. In short, the molecules i and j are defined to be H-bonded if the following polynomial function $f(d)$ is larger than 0.5 for both distances O_iO_j and $\overline{O_iH} + \overline{O_jH} - \overline{O_iO_j}$.

$$f(d) = \frac{1 - [(d - d_0)/\Delta]^n}{1 - [(d - d_0)/\Delta]^m} \quad (1)$$

where $d_0 = 2.75$, $\Delta = 0.45$, $n = 10$, and $m = 16$ if d is the O_iO_j distance and $d_0 = 0$, $\Delta = 0.4$, $n = 4$, and $m = 8$ if d is the $\overline{O_iH} + \overline{O_jH} - \overline{O_iO_j}$. When calculating the angular distributions, we include all molecules in the first solvation shell of the reference molecule, and we use 2.5 Å as the cutoff radius. This value corresponds to the position of the first intermolecular minimum of the oxygen–hydrogen radial distribution function.

We also estimate the equilibrium density predicted by different exchange–correlation functionals. To this end, we use the same approach as in ref 8. The total energies at snapshots taken from the AIMD trajectories are calculated at scaled values of the lattice constant by keeping the intramolecular coordinates fixed while rescaling the positions of the centers of mass of the water molecules. We then use the minimum of the interpolated energy values to determine the equilibrium density at a given snapshot. To sample a wide range of configurations, we use at least 30 snapshots, each separated by 100 fs. The equilibrium density quoted in Table 2 is the average over all snapshots. For this analysis, we increase the cutoff energy to 250 Ry for more reliable total energy differences in order to compensate for the fact that the basis set changes upon modifying the lattice constant.

The diffusion constant D is calculated from the slope of the mean-square displacement (MSD) curve using the Einstein relation:

$$2tD = \frac{1}{3} \langle |\mathbf{r}(t) - \mathbf{r}(t_0)|^2 \rangle \quad (2)$$

Table 2. The Average Temperature (T_{avg} , in K), the Coordination Number (n), the Average Number of H-Bonds per Water Molecule (h), the Self-Diffusion Coefficient (D , in $\text{\AA}^2/\text{ps}$), Time Constants from Orientational Autocorrelation Function ($\tau_{a,1}$ and $\tau_{a,2}$, in ps) and Their Ratio, the Estimated Equilibrium Density Relative to the Experimental One, and Characteristics of Oxygen–Oxygen Radial Distribution Function (r , in \AA ; g_{OO}) Predicted by AIMD Simulations^a

method	$T = T_{\text{avg}}$												$T = 298 \text{ K}$	
	T_{avg}	n	h	D	$\tau_{a,1}$	$\tau_{a,2}$	$\tau_{a,1}/\tau_{a,2}$	ρ/ρ_{expr}	r_{max}	$g_{\text{oo}}^{\text{max}}$	r_{min}	$g_{\text{oo}}^{\text{min}}$	$g_{\text{oo}}^{\text{max}}$	$g_{\text{oo}}^{\text{min}}$
BLYP	319	4.17	3.44	0.10	7.54	3.00	2.5	0.92	2.77	2.86	3.31	0.66	3.04	0.61
BLYP-DCACP	308	4.49	3.43	0.17	3.57	1.71	2.1	1.03	2.79	2.72	3.36	0.85	2.81	0.83
BLYP- D_{WM}	316	6.00	3.82	0.20	4.20	1.36	3.1	1.04	2.82	2.76	3.63	0.93	2.92	0.88
BLYP- D_{G2}	321	4.91	3.65	0.16	4.23	1.85	2.3	1.02	2.78	2.83	3.44	0.77	3.04	0.71
PBE	314	4.03	3.58	0.03	36.92	15.58	2.4	0.96	2.72	3.19	3.27	0.43	3.34	0.39
PBE-DCACP	323	4.06	3.63	0.05	32.73	10.04	3.3	0.97	2.71	3.27	3.28	0.40	3.49	0.33
PBE- D_{WM}	323	4.06	3.54	0.04	23.95	17.28	1.4	0.97	2.72	3.09	3.29	0.47	3.32	0.41
PBE- D_{G2}	324	4.15	3.61	0.06	23.65	8.87	2.7	1.02	2.72	3.23	3.30	0.47	3.46	0.40
revPBE	323	4.21	3.20	0.21	2.74	1.27	2.2	0.85	2.80	2.38	3.34	0.90	2.61	0.83
revPBE-DCACP	331	4.65	3.59	0.16	5.43	2.09	2.6	1.02	2.74	2.94	3.35	0.76	3.24	0.67
revPBE- D_{G2}	322	5.43	3.59	0.34	2.19	1.01	2.2	0.96	2.80	2.34	3.55	0.95	2.34	0.89
Expr	298	4.6		0.19	4.76	1.92	2.5	ref	2.74	2.76	3.39	0.79	2.76	0.79

^aThe temperature-rescaled $g_{\text{OO}}^{\text{max}}$ and $g_{\text{OO}}^{\text{min}}$ are tabulated in the last two columns, and experimental data, wherever available, are noted in the last row for comparison. The experimental values are from refs 38–40.

For improved statistics, we average the MSD curves from a series of overlapping data blocks (with different starting times t_0 and a length equal to four-fifths of the total simulation time). D is an elusive quantity to determine *in silico*. It is sensitive to the simulation protocol, including the simulation length, the pseudopotential type, and the basis set size.^{6,9,32–36} In addition, even though finite size effects are small for structural properties, they are not negligible for dynamic quantities. Size scaling is thus required for a system size of 64 water molecules to obtain a comparable value to the experimental one. Since the viscosity of heavy water is known experimentally, it is more straightforward to scale the observed (infinite-size) experimental self-diffusion coefficient to a hypothetical 64-molecule water system.

We characterize the time scale of the rotation of the molecules from the orientational autocorrelation function

$$C_{l=1,2}(t) = \frac{1}{N} \sum_i \langle P_l[\cos \theta_i(t)] \rangle \quad (3)$$

P_l is the Legendre polynomial of order l , and $\theta_i(t)$ is the angle between the direction of the water molecule i at times t and t_0 . As for the direction of a water molecule, we use the vector from the oxygen atom to the center of the two hydrogen atoms. We fit the functions $C_{l=1,2}(t)$ to the functional form $A \exp[-(t/\tau_{a,l})^\beta]$ for values in the range of 0.1–20 ps in the case of $\tau_{a,1}$ and 0.5–20 ps in the case of $\tau_{a,2}$. In addition, since the data are exponential, we weigh the data points with weighting functions $\exp(-x/5)$ and $\exp(-x)$ for $\tau_{a,1}$ and $\tau_{a,2}$, respectively. Here in this article, we only tabulate the fitted time constants $\tau_{a,1}$ and $\tau_{a,2}$; the other values are listed in the Supporting Information.

Geometries of the water clusters are optimized with gradient tolerances of 10^{-5} and 10^{-7} a.u. for the nuclear and electronic degrees of freedom, respectively. Each water cluster is centered in a cubic cell measuring 20 \AA with isolated, that is without periodic, boundary conditions using the algorithm of Hockney.³⁷

Interaction energy profiles of the dimer are evaluated as a function of the $\text{O}_\text{D}-\text{H}_\text{D}\cdots\text{O}_\text{A}$ angle ($\angle\text{OHO}$) at fixed oxygen–oxygen distances (r_{OO}). In these calculations, a water dimer is constructed by positioning two rigid monomers, whose

geometries are optimized *a priori* using the respective method, at the same C_s mirror symmetry as in the optimized water dimer. The interaction energy profile is then scanned by rotating the H-bond-donating molecule along the symmetry plane. We use quantum chemical CCSD(T) calculations as a reference. Our tests (see Supporting Information) on the effect of basis sets (aug-cc-pVnZ, n ranges from 2 to 5) show that the CCSD(T) interaction energy of the water dimer is converged to within 5 meV with the aug-cc-pV4Z basis set that we use for our reference calculations. We do not perform any basis set superposition correction in the interaction energies since these are already very well converged at this level of basis set.

3. RESULTS

3.1. Radial Distribution Functions. Oxygen–oxygen (g_{OO}) radial distribution functions evaluated from all simulations and the neutron diffraction data³⁸ are plotted in Figure 1, and some of their characteristics are tabulated in Table 2. We focus on g_{OO} here because it is least sensitive to the nuclear quantum effects that might influence the details of the structure. The oxygen–hydrogen (g_{OH}) and hydrogen–hydrogen (g_{HH}) radial distribution functions are included in the Supporting Information for completeness.

All vdW-corrected BLYP functionals predict less structured water than BLYP, as evidenced by the elevation of $g_{\text{OO}}^{\text{min}}$ and the lowering of $g_{\text{OO}}^{\text{max}}$. In particular, g_{OO} from the BLYP-DCACP simulation has the best agreement with the neutron diffraction data. In contrast, g_{OO} values from vdW-corrected PBE simulations do not differ significantly from the one predicted by PBE. Unlike BLYP and PBE, the revPBE simulation gives rise to understructured g_{OO} values compared to the neutron data. We also observe shifts toward larger radii in both r_{max} and r_{min} obtained from the revPBE simulation, as reported in ref 16. Despite being at a slightly higher average simulation temperature, g_{OO} from the revPBE-DCACP simulation is more structured than other revPBE-based ones. revPBE- D_{G2} predicts a water structure that is even softer than the already understructured revPBE water, displaying a trend opposite to the one of revPBE-DCACP.

To discard the possibility that the difference in g_{OO} is a simple manifestation of the different simulation temperatures,

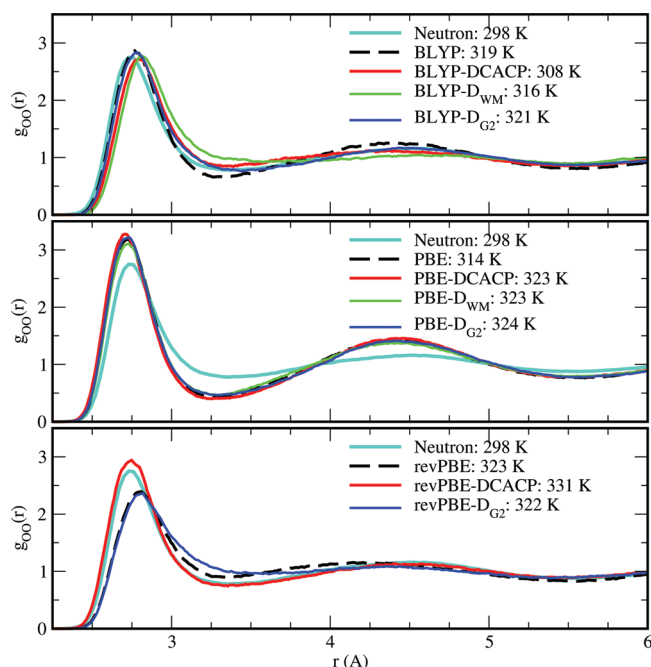


Figure 1. Oxygen–oxygen radial distribution functions (g_{OO}) of liquid water from AIMD simulations and the neutron diffraction data.³⁸ Corresponding average simulation temperatures are noted in the legend.

we rescale g_{OO}^{\min} and g_{OO}^{\max} to estimate their corresponding values at the same average temperature of 298 K, as previously described in section 2. Even after rescaling (Table 2), the trends seen in Figure 1 stay, implying that the difference is indeed due to the addition of vdW corrections.

3.2. Angular Distributions. Angular distributions of the H-bond accepting and donating water molecules are important quantities for characterizing the flexibility of H-bonds. In fact, the donor angle, $\alpha = \angle O_D-H_D \cdots O_A$, and the acceptor angle, $\theta = \angle H_D \cdots O_A-H_A$, serve as direct probes to orientational flexibility. The H-bonding angle, $\beta = \angle H_D-O_D \cdots O_A$, is the only one where an experimentally measured angular distribution is available.⁴¹ In order to make a direct comparison to experimental data, in Figure 2 we plot the distribution of the H-bonding angle $P(\beta)$ for the first solvation shell. Distributions of the donor and acceptor angles, $P(\alpha)$ and $P(\theta)$, are attached in the Supporting Information.

The positions of maxima are similar in all water models, differing by no more than a few degrees, and are consistent with a slightly bent H-bond. Nevertheless, it is still noticeable that PBE-based simulations produce narrower distributions than BLYP- and revPBE-based ones. Next, we focus on the difference within each functional family.

First, vdW-corrected BLYP simulations yield a lower probability for angles close to the maximum of $P(\beta)$ and an increased probability for larger angles consequently. $P(\beta)$ from the BLYP simulation peaks the earliest at around 8°. BLYP-DCACP and BLYP- D_{G2} functionals predict almost identical distributions whose peaks are around 9°. The BLYP- D_{WM} simulation has the broadest $P(\beta)$.

Second, the distributions predicted by PBE-based functionals show little variation among one another, and all yield too narrow $P(\beta)$ distributions, a trend that is consistent with the observation for g_{OO} .

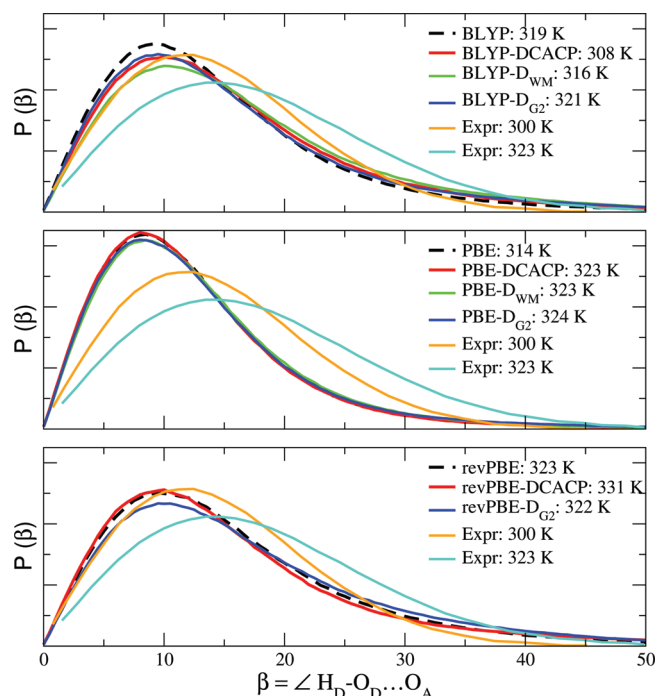


Figure 2. Distributions of the H-bonding angle β , $P(\beta)$, for the first solvation shell. Experimental values at 300 and 323 K are also shown.

Finally, based on the trend seen in g_{OO} , we expect to see a much larger difference between distributions predicted by revPBE and revPBE-DCACP than what is portrayed in Figure 2. Instead, $P(\beta)$ values from the revPBE and revPBE-DCACP simulations are almost indistinguishable. The revPBE- D_{G2} scheme, on the other hand, follows the same trend as in g_{OO} and predicts a slightly wider $P(\beta)$ than ones of revPBE and revPBE-DCACP.

In summary, all BLYP and revPBE simulations yield very similar angular distributions that are in better agreement with experimental data than the results from PBE based simulations. The inclusion of dispersion corrections does not seem to affect the angular flexibility significantly.

3.3. Coordination Numbers and H-Bond Statistics.

Classical force field simulations⁹ have shown that an increase of 53 K in temperature alters the coordination number, n , by 0.2 at most (albeit much less in most cases). They have also reported only a small change in n between AIMD simulations (BLYP functional) at 300 and 353 K. As a result, we can safely assume that the temperature dependence in n is very small, and the changes in n (ranging from 4 to 6, see Table 2) are indeed due to the changes in the intermolecular interactions.

Nevertheless, the large n values from the revPBE- D_{G2} and BLYP- D_{WM} simulations appear unphysical. We conclude that this is simply a consequence of our inflexible rule of assigning r_{\min} as the upper bound of the integration in the definition of n . Indeed, the values of n with different functionals and vdW corrections show a strong linear correlation with r_{\min} . Thus, in the cases where g_{OO} is understructured, the value of r_{\min} is considerably larger, resulting in a much larger n . Therefore, the changes in the value of n between different functionals do not contain any information beyond r_{\min} , and we do not discuss it further here.

Also tabulated in Table 2 are the average numbers of H-bonds, h . First, we note that even though h varies from 3.2 to 3.8, none of the simulations challenges the concept that liquid

water is tetrahedrally coordinated, a recent dispute concerning water. Second, there is a large increase in h going from BLYP to BLYP- D_{WM} , from BLYP to BLYP- D_{G2} , and from revPBE to revPBE- D_{G2} . Going from BLYP to BLYP-DCACP introduces little change in h , deviating from the trend of increased h due to the addition of vdW corrections.

Consistent with the results on radial and angular distributions, irrespective of whether vdW corrections are applied or not, the change in h is very small across PBE-based simulations and BLYP vs BLYP-DCACP.

3.4. Density of Liquid Water. Owing to the shortcomings of the pure GGA functionals, the interactions between molecules in liquid water are not properly described. As a result, the predicted density deviates from the (experimental) equilibrium value.^{8,15,16} Nevertheless, including corrections for vdW effects improves the prediction of the equilibrium density. A density of 0.8 g cm^{-3} , 20% smaller than in experiments, was found with the pure BLYP functional using DFT-based isobaric–isothermal Monte Carlo simulations.⁸ A similar value was obtained using AIMD simulations within the NPT ensemble, and the prediction was improved to within 1% of the experimental value with the BLYP- D_{G2} approximation.¹⁵ Similar improvement was found going from PBE to PBE- D_{G2} . In addition, simulations of a vapor–liquid interface within the NVT ensemble using BLYP and BLYP- D_{G2} gave the same trend for the density in the middle of the water slab.⁴² Ref 16 reported a trend, $\rho_{\text{revPBE}} < \rho_{\text{BLYP}} < \rho_{\text{PBE}} < \rho_{\text{exp}}$, with the pure density functionals, and a density close to, or even slightly higher, than experimental values with a vdW-density functional.⁴³

Our estimated densities (see Table 2) follow the same trend as seen in previous works. The pure GGA functionals all underestimate the density, whereas all vdW-corrected schemes lead to improved densities close to the experimental value. Our results also agree with the corresponding trend in ice.⁴⁴

3.5. Self-Diffusion Coefficients. In Figure 3, we plot the self-diffusion coefficients, D , versus temperature for different

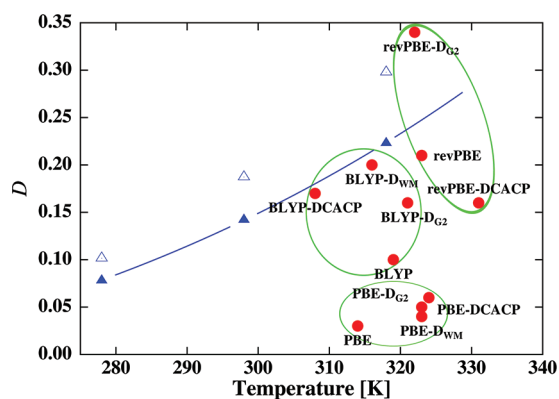


Figure 3. Estimated self-diffusion coefficients, D , in $\text{\AA}^2/\text{ps}$, versus average simulation temperatures. The observed experimental values for heavy water³⁹ and the corresponding values after adjusting for finite size effects are marked by empty and filled triangles, respectively. The lines are guides for the eye.

functionals together with both the observed and the finite size-rescaled experimental data for heavy water. D predicted by the BLYP functional is considerably lower than the experimental data, whereas D calculated from the BLYP-DCACP and BLYP- D_{WM} simulations are in excellent agreement with the scaled

experimental D . The PBE functional yields a value of D that is far too low.^{32,35} Even after adding vdW corrections to it, the predicted D values do not improve and remain too low. D calculated from the revPBE trajectory, on the other hand, is already quite close to the scaled experimental data. The revPBE- D_{G2} scheme predicts a coefficient that is larger than the observed experimental value. As for other properties previously considered, the best (among the functionals considered here) description of the self-diffusion of water is achieved with BLYP-DCACP.

3.6. Orientational Self-Correlation. The orientational autocorrelation function gives information about the reorientation time of the water molecules in the liquid. In Table 2, we show also the values for the time constants $\tau_{a,1}$ and $\tau_{a,2}$ together with the experimentally derived times.⁴⁰ We note that the experiments were measured at temperature of 300 K. Thus, the values derived from our simulations would be somewhat lower.

The trend of the time constants agrees well with the observations in other quantities above: Where the diffusion is slow and the radial distribution functions overstructured, the $\tau_{a,i}$ are larger and vice versa. In particular, the values for all variants of the PBE functional are too large, and only few rotations of a given molecule occur within our extended simulations. vdW corrections to the BLYP functional result in a decrease of the orientational correlation, bringing the two time constants closer to the experimentally derived values. revPBE-DCACP opposes the trend seen in going from revPBE to revPBE- D_{G2} . We again attribute this controversy to the very large DCACP correction for the hydrogen in this case.

We also list the ratio $\tau_{a,1}/\tau_{a,2}$ in Table 2. Despite relatively large variations in the time constants themselves, the ratios differ by a much smaller amount. The values of $\tau_{a,1}$ and $\tau_{a,2}$ obtained from the PBE-based simulations, however, are comparable to the simulation length and therefore cannot be considered as converged. As discussed in ref 45 and references therein, a value of the ratio $\tau_{a,1}/\tau_{a,2}$ close to 3 would correspond to standard rotational diffusion occurring during the dynamics. In most cases, we, however, obtain values in Table 2 that are closer to 2 than 3, which rather supports the “jump diffusion” model put forward by Laage and Hynes using classical molecular dynamics simulations.^{46,47} The only clear exception to this systematics is the BLYP- D_{WM} approach, which, nonetheless, yields overly diffusive and understructured water.

3.7. Cluster Studies. While some characteristics of liquid water remain controversial, the gas-phase water-cluster community has provided a consistent experimental and theoretical picture of the behaviors of small water clusters.^{48–50} By comparing with these data, we hope to shed light on the different performances offered by the functionals we tested in this study.

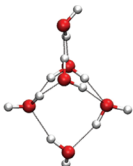
Interaction energies and geometries of geometry-optimized water clusters (dimer to hexamers) from our calculations are tabulated in Tables 3 and 4, and in Table 5 we summarize the average, smallest, and largest differences. Apart from BLYP, revPBE, and revPBE- D_{G2} , all other methods consistently overbind compared to the MP2 results at the complete basis set limit (MP2/CBS).⁴⁸ revPBE, in particular, predicts the weakest H-bonds. Surprisingly, PBE gives the best results even though its liquid water is grossly overstructured. Adding vdW corrections to BLYP improves its performance, and estimates from the BLYP-DCACP and BLYP- D_{G2} functional are on par

Table 3. Interaction Energy (E_{int} in eV), Interaction Energy per H-Bond (e_{int} in eV), Average O–O Distance ($\langle r \rangle$, in Å), and Average Donor Angle ($\langle \alpha \rangle$, in Degrees; $\alpha = \angle_{\text{OD-HD}\cdots\text{OA}}$) of Optimized Water Clusters from Dimer to Pentamer^a

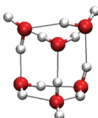
dimer				trimer				tetramer				cyclic pentamer			
	E_{int}	r	α	E_{int}	e_{int}	$\langle r \rangle$	$\langle \alpha \rangle$	E_{int}	e_{int}	$\langle r \rangle$	$\langle \alpha \rangle$	E_{int}	e_{int}	$\langle r \rangle$	$\langle \alpha \rangle$
BLYP	-0.183	2.93	171.2	-0.571	-0.190	2.84	151.0	-1.052	-0.263	2.79	167.9	-1.393	-0.279	2.74	175.8
BLYP-DCACP	-0.230	2.92	170.3	-0.722	-0.241	2.81	151.1	-1.289	-0.322	2.75	168.3	-1.686	-0.337	2.72	176.3
BLYP-D _{WM}	-0.242	2.92	170.6	-0.738	-0.246	2.84	150.5	-1.314	-0.328	2.79	167.7	-1.720	-0.344	2.75	175.9
BLYP-D _{G2}	-0.224	2.91	168.3	-0.721	-0.240	2.81	151.9	-1.273	-0.318	2.74	169.1	-1.658	-0.332	2.72	177.0
PBE	-0.219	2.91	171.0	-0.698	-0.233	2.79	152.2	-1.260	-0.315	2.73	168.7	-1.665	-0.333	2.70	176.5
PBE-DCACP	-0.226	2.88	170.6	-0.724	-0.241	2.78	152.2	-1.299	-0.325	2.72	168.6	-1.716	-0.343	2.69	176.4
PBE-D _{WM}	-0.279	2.88	170.6	-0.865	-0.288	2.80	151.7	-1.519	-0.380	2.73	168.3	-1.986	-0.397	2.72	176.5
PBE-D _{G2}	-0.247	2.88	168.8	-0.797	-0.266	2.78	152.5	-1.409	-0.352	2.71	169.4	-1.845	-0.369	2.68	177.3
revPBE	-0.153	2.99	171.4	-0.475	-0.158	2.85	151.4	-0.902	-0.225	2.77	168.2	-1.207	-0.241	2.76	176.4
revPBE-DCACP	-0.247	2.87	166.8	-0.829	-0.276	2.76	153.6	-1.407	-0.352	2.72	170.1	-1.809	-0.362	2.70	177.5
revPBE-D _{G2}	-0.183	2.89	167.7	-0.599	-0.200	2.81	152.2	-1.088	-0.272	2.76	169.5	-1.423	-0.285	2.74	177.3
MP2/CBS ⁴⁸	-0.216	2.91	–	-0.686	-0.229	2.79	–	-1.198	-0.299	2.73	–	-1.573	-0.315	–	–

^aThe magnitude of the difference, $\Delta e_{\text{int}} = e_{\text{int}}^{\text{XC}} - e_{\text{int}}^{\text{MP2}}$, is color-coded: $\Delta e_{\text{int}} < -0.03$ in red, $\Delta e_{\text{int}} > +0.03$ in cyan.

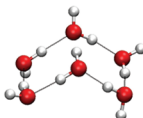
Table 4. Interaction Energy (E_{int} in eV), Interaction Energy Per H-Bond (e_{int} in eV), Average O–O Distance ($\langle r \rangle$, in Å), and Average Donor Angle ($\langle \alpha \rangle$, in Degrees; $\alpha = \angle_{\text{OD-HD}\cdots\text{OA}}$) of Optimized Water Hexamers^a



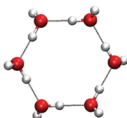
cage hexamer



prism hexamer



book hexamer



cyclic hexamer

	E_{int}	e_{int}	$\langle r \rangle$	$\langle \alpha \rangle$	E_{int}	e_{int}	$\langle r \rangle$	$\langle \alpha \rangle$	E_{int}	e_{int}	$\langle r \rangle$	$\langle \alpha \rangle$	E_{int}	e_{int}	$\langle r_{\text{OO}} \rangle$	$\langle \alpha \rangle$
BLYP	-1.644	-0.205	2.86	159.1	-1.630	-0.181	2.88	152.9	-1.724	-0.282	2.76	168.5	-1.694	-0.287	2.73	178.3
BLYP-DCACP	-2.160	-0.270	2.81	159.2	-2.173	-0.241	2.83	153.1	-2.129	-0.355	2.73	168.8	-2.057	-0.343	2.72	177.9
BLYP-D _{WM}	-2.220	-0.278	2.82	159.2	-2.250	-0.250	2.84	153.1	-2.181	-0.363	2.77	168.3	-2.109	-0.352	2.75	177.6
BLYP-D _{G2}	-2.109	-0.264	2.80	160.2	-2.123	-0.236	2.83	154.0	-2.086	-0.348	2.73	169.6	-2.026	-0.338	2.72	177.4
PBE	-2.017	-0.252	2.81	159.7	-2.011	-0.223	2.84	153.5	-2.053	-0.342	2.72	169.1	-2.053	-0.342	2.69	177.4
PBE-DCACP	-2.082	-0.260	2.78	159.4	-2.076	-0.231	2.83	153.5	-2.118	-0.353	2.71	169.0	-2.115	-0.352	2.69	177.5
PBE-D _{WM}	-2.615	-0.327	2.77	159.8	-2.646	-0.294	2.80	153.6	-2.541	-0.423	2.73	168.9	-2.429	-0.405	2.70	177.1
PBE-D _{G2}	-2.332	-0.291	2.76	160.2	-2.338	-0.260	2.80	154.2	-2.318	-0.386	2.69	169.8	-2.257	-0.376	2.68	176.9
revPBE	-1.382	-0.173	2.88	159.4	-1.366	-0.152	2.92	153.0	-1.450	-0.242	2.78	169.0	-1.493	-0.249	2.74	177.5
revPBE-DCACP	-2.395	-0.299	2.73	161.2	-2.411	-0.268	2.76	154.8	-2.311	-0.385	2.69	170.4	-2.214	-0.369	2.69	176.6
revPBE-D _{G2}	-1.760	-0.220	2.84	160.5	-1.764	-0.196	2.87	154.0	-1.768	-0.295	2.74	169.7	-1.743	-0.291	2.70	176.9
MP2/CBS	-1.990	-0.249	—	—	-1.988	-0.221	—	—	-1.978	-0.330	—	—	-1.943	-0.324	—	—
DMC ⁵¹	-1.977	-0.247	—	—	-1.991	-0.221	—	—	-1.967	-0.328	—	—	-1.925	-0.321	—	—
CCSD(T) ⁵²	-2.073	-0.259	—	—	-2.086	-0.232	—	—	-2.033	-0.339	—	—	-1.995	-0.333	—	—

^aThe magnitude of the difference, $\Delta e_{\text{int}} = e_{\text{int}}^{\text{XC}} - e_{\text{int}}^{\text{MP2}}$, is color-coded: $\Delta e_{\text{int}} < -0.03$ in red, $\Delta e_{\text{int}} > +0.03$ in cyan.

Table 5. Average, Smallest, and Largest (in Absolute Value) Difference in Interaction Energy per H-Bond (e_{int} in eV) Relative to the MP2/CBS Results in the Water Clusters from Dimer to Hexamer^a

	$\overline{(\Delta e_{\text{int}})}$	$(\Delta e_{\text{int}})_{\text{min}}$	$(\Delta e_{\text{int}})_{\text{max}}$
BLYP	+0.039	+0.033	+0.048
BLYP-DCACP	-0.020	-0.012	-0.025
BLYP-D _{WM}	-0.028	-0.017	-0.033
BLYP-D _{G2}	-0.015	-0.008	-0.019
PBE	-0.010	-0.002	-0.018
PBE-DCACP	-0.019	-0.010	-0.028
PBE-D _{WM}	-0.076	-0.059	-0.093
PBE-D _{G2}	-0.046	-0.031	-0.056
revPBE	+0.074	+0.063	+0.088
revPBE-DCACP	-0.047	-0.031	-0.055
revPBE-D _{G2}	+0.030	+0.025	+0.033

^aThe magnitude of the difference $\Delta e_{\text{int}} = e_{\text{int}}^{\text{XC}} - e_{\text{int}}^{\text{MP2}}$ is illustrated with a color code: $\Delta e_{\text{int}} < -0.03$ in red, $\Delta e_{\text{int}} > +0.03$ in cyan.

with the ones of PBE. The BLYP-DCACP thus describes both the liquid and the H-bonds in the clusters well.

To further evaluate the accuracy of the different combinations of the exchange-correlation functionals with various vdW-correction schemes, we analyze the angular dependence of the interaction energy profiles in a water dimer. This allows us to

probe situations close to the H-bonding configuration (i.e., small values of H-bonding angle, β) and repulsive arrangements (β closer to 180°). Figure 4 shows the deviation of the interaction energy from the reference curve, ΔE_{int} , as a function of β . (The full interaction energy profiles are provided in the Supporting Information.) We use the highly accurate quantum-chemical CCSD(T)/aug-cc-pV4Z method to calculate the reference curve. The energies are calculated for the different functionals with and without vdW corrections at an O–O distance of 2.75 Å, which represents the maximum of the radial distribution functions, or the distance where the hydrogen bond is at its strongest.

The BLYP dimer consistently binds too weakly, and its ΔE_{int} has a small angular dependence. In this case, functionals with vdW corrections, which are quite isotropic with respect to the rotation of a water molecule, yield a relatively constant shift to the interaction energy profile, and the resulting interaction energy profiles are in very good agreement with the reference calculation.

The results from the PBE functionals are also relatively close to the reference, but at small angles (i.e., the H-bonding configuration) the dimer is clearly overbinding relative to angles greater than, say, 60° . This will no doubt give a strong bias toward the configurations with H-bonding. Indeed, the

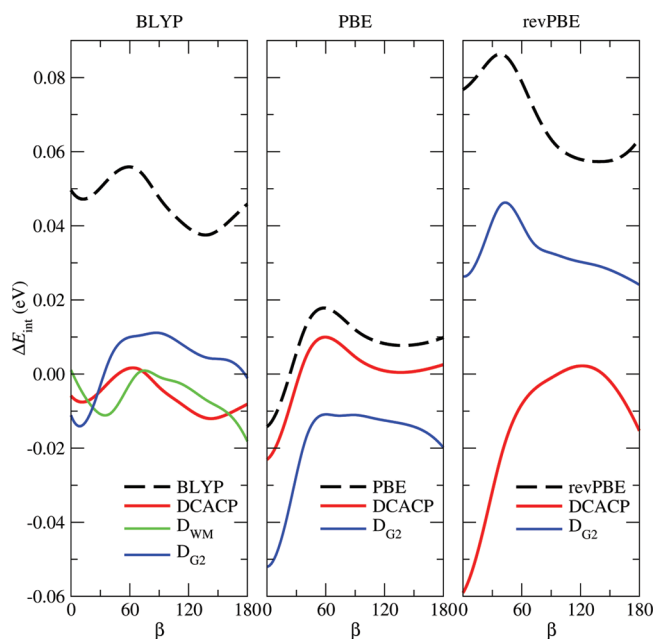


Figure 4. Difference of the interaction energy from the CCSD(T) reference calculation, $\Delta E_{\text{int}} = E_{\text{int}}^{\text{XC}} - E_{\text{int}}^{\text{CCSD(T)}}$, of two fixed water monomers at an O–O distance of 2.75 Å as a function of the H-bonding angle β .

radial distribution functions are overstructured and the diffusion constants of the liquid too low. The vdW corrections do not change the angular dependence, but the PBE- D_{G2} dimer binds too strongly.

The revPBE dimer binds consistently too little, and the error is largest at small angles, close to the direction of the H-bond. Adding the D_{G2} vdW correction shifts the curve toward the reference curve, and the error in the region of small angles is reduced. The revPBE-DCACP, however, leads to a very large preference for H-bonds, a possible reason why the liquid water from the revPBE-DCACP simulations is much more structured than the ones from revPBE and revPBE- D_{G2} simulations.

4. DISCUSSION

The bare BLYP functional in which the dispersion force is entirely absent predicts positive interaction energies for all vdW-dominated complexes such as rare-gas and hydrogen dimers.^{53–58} The PBE functional, on the other hand, is rather system-dependent and shows spurious attractive interactions for some vdW-bound systems. For example, the interaction energy of $(\text{H}_2)_2$, the calibration system for hydrogen DCACP, estimated by PBE is overbinding with respect to the reference calculation with the full configuration interaction method. As a consequence, DCACPs complementing BLYP always provide an attractive correction to the underlying functional, in line with the idea of a dispersion-motivated correction. The DCACP parameters for PBE, however, can be repulsive (hydrogen and helium) or attractive (carbon, nitrogen, oxygen, etc.). In addition, the deviation in the angular dependence of the interaction energy with PBE from the high-level calculations cannot be efficiently compensated by adding either the empirical vdW corrections (that are purely radial-dependent in general) or the DCACPs (whose corrections are only very weakly angular-dependent).

Adding vdW corrections to the BLYP functional always improves the energetics and the geometries of the water

clusters. This improvement manifests itself in the liquid simulations, resulting in a softening of the intermolecular interactions and an increase in mobility that is in good agreement with the experiments (see Figure 3). As for the oxygen–oxygen radial distribution function, the best agreements are obtained with the DCACP and D_{G2} schemes (cf. Figure 1).

In contrast, the PBE functional as well as its vdW-corrected variants show a much more reduced transferability to a large range of bonding geometries. The spurious part of the vdW interactions depends strongly on the actual overlap of the electronic density and, as a result, leads to unpredictable contributions. While the PBE geometry-optimized clusters and the estimated dimer interaction energy profiles agree very well with high-level *ab initio* calculations [MP2/CBS or CCSD(T)/aug-cc-pV4Z level of theory], the predicted properties of PBE liquid water are rather dismal. PBE water is too structured, as shown by the radial and angular distribution functions (Figures 1 and 2), and all dynamical properties investigated are too slow (a very small diffusion coefficient), even more so than the bare BLYP water. Augmenting PBE with either DCACPs or empirical vdW corrections only changes the interaction energy profiles of the water dimer and the equilibrium energies of the water clusters by a very small amount, without necessarily improving the PBE results. In general, vdW-corrected PBE functionals seem unable to capture the right balance between H-bonded and vdW interactions, leading to a deterioration of the structural and dynamical properties of water clusters and liquid.

In a recent study on liquid water,¹⁷ accurate structural and dynamical properties that are close to the experimental results were obtained using the vdW density functional (vdW-DF) with the PBE exchange plus a local density approximation (LDA) and a nonlocal correlation terms (see ref 43 for a detailed review). The vdW-DF study suggests that the difficulties that we have encountered in adding vdW interactions to PBE are mainly due to an incompatibility (a kind of “double counting”) with the correlation part. Nevertheless, this is not entirely due to the spurious attractive nature of the PBE correlation, since the vdW-DF correction is based on the (in general) even more attractive LDA correlation.

Finally, results from vdW-corrected revPBE functionals show once more how difficult it is to conciliate the results from cluster simulations with the ones from the liquid phase. In general, the performance of vdW-corrected revPBE functionals in the cluster calculations are quite poor: revPBE- D_{G2} underbinds all structures (improving, but only slightly, the bare revPBE results), while revPBE-DCACP overbinds. We think that in the case of the DCACP correction, the exceptionally large correction strength σ_1 for the hydrogen atom (see Table 1) is responsible for this behavior. On the other hand, revPBE- D_{G2} gives a clearly understructured g_{OO} for the liquid, while the DCACP correction produces a g_{OO} that can hardly be distinguished from the neutron diffraction data (except for the different height at the first peak; see Figure 1). We, however, do not want to claim that revPBE-DCACP is the corrected functional to be used in DFT-based simulations of liquid water but to simply observe how a somewhat “unphysical” strengthening of the intermolecular O–H interactions can affect the overall liquid phase structure without improving its dynamical properties (cf. Figure 3).

5. CONCLUSIONS

We have carried out AIMD simulations of liquid water using density functional theory with three GGA functionals. Two empirical approaches, DCACPs and pair-potential based vdW corrections, are employed to compensate for the fact that London dispersion forces are not described in DFT-GGAs. We note that this problem persists in DFT-hybrid functionals, where only the exchange functional has been modified.

All results for structural and dynamical properties point to much more glass-like liquid water with PBE, even when compared to the already overstructured BLYP water. Furthermore, unlike BLYP in which the addition of either DCACPs or empirical vdW corrections leads to accurate interaction energies in water clusters and a softer liquid structure, augmenting PBE with either of the two does not resolve the discrepancy. It is likely that the “spurious” behavior of PBE in treating dispersion forces renders the corresponding DCACPs less transferable than the ones for BLYP, where the contribution of DCACPs is much more clear-cut. The bare revPBE functional provides relatively good results for the liquid, even though it underbinds in water clusters. The opposing trend from the two different vdW-correction schemes shows how careful one has to be in treating weak interactions. Overall, we find that the best agreement with the experiments is obtained using the BLYP functional in combination with dispersion corrections as either the BLYP-DCACP or BLYP-D_{G2} variant.

We are convinced that a proper treatment of vdW interactions is essential in liquid water simulations, not only for a better description of its properties but, more importantly, for studying the many phenomena occurring in wet environments, such as hydrophobicity.

■ ASSOCIATED CONTENT

Supporting Information

Convergence test on cutoff energy, details on the simulation trajectories, more radial and angular distribution functions, mean-square displacements, power spectra, and vibrational frequencies of small water clusters.

This material is available free of charge via the Internet at <http://pubs.acs.org/>.

■ AUTHOR INFORMATION

Corresponding Author

*E-mail: Ari.P.Seitsonen@iki.fi.

Present Address

^{||}Center for Neural Science, New York University, 4 Washington Place, New York, New York 10003, United States

Notes

The authors declare no competing financial interest.

■ ACKNOWLEDGMENTS

We acknowledge Mauricio D Coutinho-Neto for many useful discussions. I-C.L. thanks the Swiss National Science Foundation (PBELP2-123062) for its financial support. U.R. gratefully acknowledges support from Swiss NSF Grant No. 200020-130082 and the NCCR-MUST interdisciplinary research program.

■ REFERENCES

- (1) Hohenberg, P.; Kohn, W. *Phys. Rev.* **1964**, *136*, B864.
- (2) Kohn, W.; Sham, L. J. *Phys. Rev.* **1965**, *140*, A1133.
- (3) Becke, A. D. *Phys. Rev. A* **1988**, *38*, 3098.
- (4) Lee, C.; Yang, W.; Parr, R. G. *Phys. Rev. B* **1988**, *37*, 785.
- (5) Perdew, J. P.; Burke, K.; Ernzerhof, M. *Phys. Rev. Lett.* **1996**, *77*, 3865.
- (6) Kuo, I. W.; Mundy, C. J.; McGrath, M. J.; Siepmann, J. I.; VandeVondele, J.; Sprik, M.; Hutter, J.; Chen, B.; Klein, M. L.; Mohamed, F.; Krack, M.; Parrinello, M. *J. Phys. Chem. B* **2004**, *108*, 12990.
- (7) VandeVondele, J.; Mohamed, F.; Krack, M.; Hutter, J.; Sprik, M.; Parrinello, M. *J. Chem. Phys.* **2005**, *122*, 014515.
- (8) McGrath, M. J.; Siepmann, J. I.; Kuo, I. W.; Mundy, C. J.; VandeVondele, J.; Hutter, J.; Mohamed, F.; Krack, M. *Chem. Phys. Chem.* **2005**, *6*, 1894.
- (9) Mantz, Y. A.; Chen, B.; Martyna, G. J. *J. Phys. Chem. B* **2006**, *110*, 3540.
- (10) Kühne, T. D.; Krack, M.; Parrinello, M. *J. Chem. Theory Comput.* **2009**, *5*, 235.
- (11) Cho, C. H.; Singh, S.; Robinson, G. W. *J. Chem. Phys.* **1997**, *107*, 7979.
- (12) Schmid, R. *Monatsh. Chem.* **2001**, *132*, 1295.
- (13) Lynden-Bell, R. M.; Debenedetti, P. G. *J. Phys. Chem. B* **2005**, *109*, 6527.
- (14) Lin, I.-C.; Seitsonen, A. P.; Tavernelli, I.; Coutinho-Neto, M. D.; Rothlisberger, U. *J. Phys. Chem. B* **2008**, *113*, 1127.
- (15) Schmidt, J.; VandeVondele, J.; Kuo, I.-F. W.; Sebastiani, D.; Siepmann, J. I.; Hutter, J.; Mundy, C. J. *J. Phys. Chem. B* **2009**, *113*, 11959.
- (16) Wang, J.; Román-Pérez, G.; Soler, J. M.; Artacho, E.; Fernández-Serra, M.-V. *J. Chem. Phys.* **2010**, *134*, 024516.
- (17) Zhang, C.; Wu, J.; Galli, G.; Gygi, F. *J. Chem. Theory Comput.* **2011**, *7*, 3054.
- (18) Møgelhøj, A.; Kelkkanen, A. K.; Wikfeldt, K. T.; Schiøtz, J.; Mortensen, J. J.; Pettersson, L. G. M.; Lundqvist, B. I.; Jacobsen, K. W.; Nilsson, A.; Nørskov, J. K. *J. Phys. Chem. B* **2011**, *115*, 14149–14160.
- (19) Jonchiere, R.; Seitsonen, A. P.; Ferlat, G.; Saitta, A. M.; Vuilleumier, R. *J. Chem. Phys.* **2012**, *135*, 154503.
- (20) Remsing, R. C.; Rodgers, J. M.; Weeks, J. D. *J. Stat. Phys.* **2011**, *145*, 313.
- (21) Car, R.; Parrinello, M. *Phys. Rev. Lett.* **1985**, *55*, 2471.
- (22) Zhang, Y.; Yang, W. *Phys. Rev. Lett.* **1998**, *80*, 890.
- (23) von Lilienfeld, O. A.; Tavernelli, I.; Rothlisberger, U.; Sebastiani, D. *Phys. Rev. Lett.* **2004**, *93*, 153004.
- (24) Grimme, S. *J. Comput. Chem.* **2006**, *27*, 1787.
- (25) Williams, R. W.; Malhotra, D. *Chem. Phys.* **2006**, *327*, 54.
- (26) CPMD, version 3.11; IBM Corp.: Armonk, NY, 1990–2006; MPI für Festkörperforschung Stuttgart: Stuttgart, Germany, 1997–2001. <http://www.cpmc.org> (accessed June 2012).
- (27) Goedecker, S.; Teter, M.; Hutter, J. *Phys. Rev. B* **1996**, *54*, 1703.
- (28) Lin, I.-C.; Coutinho-Neto, M. D.; Felsenheimer, C.; von Lilienfeld, O. A.; Tavernelli, I.; Rothlisberger, U. *Phys. Rev. B* **2007**, *75*, 205131.
- (29) Hutter, J. Private communication.
- (30) Hura, G.; Russo, D.; Glaeser, R. M.; Head-Gordon, T.; Krack, M.; Parrinello, M. *Phys. Chem. Chem. Phys.* **2003**, *5*, 1981.
- (31) Raiteri, P.; Laio, A.; Parrinello, M. *Phys. Rev. Lett.* **2004**, *93*, 087801.
- (32) Grossman, J. C.; Schwegler, E.; Draeger, E. W.; Gygi, F.; Galli, G. *J. Chem. Phys.* **2004**, *120*, 300.
- (33) Fernández-Serra, M. V.; Artacho, E. *Phys. Rev. Lett.* **2006**, *96*, 016404.
- (34) Sit, P. H.-L.; Marzari, N. *J. Chem. Phys.* **2005**, *122*, 204510.
- (35) Todorova, T.; Seitsonen, A. P.; Hutter, J.; Kuo, I. W.; Mundy, C. J. *J. Phys. Chem. B* **2006**, *110*, 3685.
- (36) Lee, H.-S.; Tuckerman, M. E. *J. Chem. Phys.* **2007**, *126*, 164501.
- (37) Hockney, R. W. *Methods Comput. Phys.* **1970**, *9*, 136.
- (38) Soper, A. K. *Chem. Phys.* **2000**, *258*, 121.
- (39) Mills, R. J. *Phys. Chem.* **1973**, *77*, 685.

- (40) Sansom, M. S. P.; Kerr, I. D.; Breed, J.; Sankararamakrishnan, R. *Biophys. J.* **1996**, 70, 693.
- (41) Modig, K.; Pfrommer, B. G.; Halle, B. *Phys. Rev. Lett.* **2003**, 90, 075502.
- (42) Baer, M. D.; Mundy, C. J.; McGrath, M. J.; Kuo, I.-F. W.; Siepmann, J. I.; Tobias, D. J. *J. Chem. Phys.* **2011**, 135, 124712.
- (43) Langreth, D. C.; et al. *J. Phys.: Condens. Matter* **2009**, 21, 084203.
- (44) Remsing, R. C.; Rodgers, J. M.; Weeks, J. D. *J. Stat. Phys.* **2011**, 145, 313.
- (45) Laage, D. *J. Phys. Chem. B* **2009**, 113, 2684.
- (46) Laage, D.; Hynes, J. T. *Science* **2006**, 311, 832.
- (47) Laage, D.; Hynes, J. T. *J. Phys. Chem. B* **2008**, 112, 14230.
- (48) Xantheas, S. S.; Burnham, C. J.; Harrison, R. G. *J. Chem. Phys.* **2002**, 116, 1493.
- (49) Silvestrelli, P. L. *Chem. Phys. Lett.* **2009**, 475, 285.
- (50) Kelkkanen, A. K.; Lundqvist, B. I.; Nørskov, J. K. *J. Chem. Phys.* **2009**, 131, 046102.
- (51) Santra, B.; Michaelides, A.; Fuchs, M.; Tkatchenko, A.; Flippi, C.; Scheffler, M. *J. Chem. Phys.* **2008**, 129, 194111.
- (52) Olson, R. M.; Bentz, J. L.; Kendall, R. A.; Schmidt, M. W.; Gordon, M. S. *J. Chem. Theory Comput.* **2007**, 3, 1312.
- (53) Kristyán, S.; Pulay, P. *Chem. Phys. Lett.* **1994**, 229, 175.
- (54) Pérez-Jordá, J. M.; Becke, A. D. *Chem. Phys. Lett.* **1995**, 233, 134.
- (55) Zhang, Y.; Pan, W.; Yang, W. *J. Chem. Phys.* **1997**, 107, 7921.
- (56) Patton, D. C.; Pederson, M. R. *Int. J. Quantum Chem.* **1998**, 69, 619.
- (57) van Mourik, T.; Gdanitz, R. J. *J. Chem. Phys.* **2002**, 116, 9620.
- (58) Tao, J.; Perdew, J. P. *J. Chem. Phys.* **2005**, 122, 114102.